AGU PUBLICATIONS

JGR

Journal of Geophysical Research: Oceans

RESEARCH ARTICLE

10.1002/2016JC011693

An observations and model-based analysis of meridional transports in the South Atlantic

Sudip Majumder[1,2], Claudia Schmid[2], and George Halliwell[2]

[1]Cooperative Institute for Marine and Atmospheric Studies, University of Miami, Miami, Florida, USA, [2]Atlantic Oceanographic and Meteorological Laboratory, National Oceanic and Atmospheric Administration, Miami, Florida, USA

Key Points:
- Argo observations and sea surface heights are used to estimate meridional overturning volume and heat transports in the South Atlantic
- Mean meridional volume and heat transports in the observations are higher than the estimates derived from three data assimilative models
- Observations show about the same change in meridional heat transport for 1 SV change in volume transport across 25°S, 30°S, and 35°S

Correspondence to:
S. Majumder,
sudip.majumder@noaa.gov.

Citation:
Majumder, S., C. Schmid, and G. Halliwell (2016), An observations and model-based analysis of meridional transports in the South Atlantic, *J. Geophys. Res. Oceans*, *121*, 5622–5638, doi:10.1002/2016JC011693.

Received 2 FEB 2016
Accepted 11 JUL 2016
Accepted article online 13 JUL 2016
Published online 6 AUG 2016

Abstract A three-dimensional velocity field constructed from Argo observations and sea surface heights (called Argo and SSH, hereinafter) is used to estimate meridional overturning volume transport and meridional heat transport (MHT) across 20°S, 25°S, 30°S, and 35°S for the years 2000–2014 in the South Atlantic. Volume transport in the upper branch of Meridional Overturning Circulation (MOC) and MHT from the observations are consistent with the previous observations, but are higher than the estimates derived from three data assimilative ocean models, at some of the latitudes. Both the observations and models show strong correlations between the strength of MOC and MHT at all the latitudes. The corresponding change in MHT for 1 Sv change of MOC strength, in the observations, increases from 0.046 PW in 25°S, 30°S, and 35°S to 0.056 PW across 20°S. A comparison of model-based transports at 35°S at the boundaries and in the interior with those from Argo and SSH shows significant differences between them with respect to the contributions in the three segments of the section. In addition, the contributions also vary greatly between the different models. An analysis of the seasonality of MOC in the models and in the observations reveals that MOC anomalies in the models mostly show strong annual cycles at all the latitudes, whereas those derived from Argo and SSH exhibit annual cycles at three latitudes (35°S, 30°S, and to a lesser extent at 25°S) and a semiannual cycle at 20°S.

1. Introduction

The Atlantic Meridional Overturning Circulation (MOC), consisting of a northward flow of warm water in the upper layer and southward flow of cold water in the deeper layers, plays an important role in the global energy balance [e.g., *Talley*, 2003].

The Atlantic MOC transfers heat from the tropics and southern hemisphere to the north, and is believed to be linked to several climate phenomena such as past climate change, hurricane intensity in the North Atlantic [e.g., *Vellinga and Wood*, 2002; *Stouffer et al*., 2006], anthropogenic climate forcing [*Broecker*, 1997], and changes in the monsoon rain fall pattern in the African and Indian subcontinent [*Enfield et al*., 2000; *Sutton and Hodson*, 2005], as well as global monsoon variability [*Lopez et al*., 2016].

The variability of the MOC is extensively studied in the North Atlantic [e.g., *Cunningham et al*., 2007; *Chidichimo et al*., 2010; *Hobbs and Willis*, 2012; *McCarthy et al*., 2012; *Johns*, 2011] due to the relatively large amount of observations available in this region. Even though the South Atlantic plays an important role by transporting heat from the south toward the equator, and includes large areas where water masses from different oceans mix [e.g., *Gordon*, 1985, 1986; *Garzoli and Matano*, 2011], this ocean is historically poorly sampled.

Previous studies [e.g., *de las Heras and Schlitzer*, 1999; *Saunders and King*, 1995; *Fu*, 1981, Table 1] in the South Atlantic found that the meridional heat transport (MHT) ranges from -0.23 PW ($1\ \text{PW} = 10^{15}$ W) at 30°S [*de las Heras and Schlitzer*, 1999] (using inverse model and observations) to 0.94 PW at 45°S (direct method) [*Saunders and King*, 1995]. *Ganachaud and Wunsch* [2003] used CTD observations in conjunction with annual mean NCEP climatological winds and found a MHT of 0.4 PW at 30°S. *McDonagh and King* [2005] recalculated the MHT across 30°S (World Ocean Circulation Experiment Section A10) using a box inverse model and obtained a value of 0.22 ± 0.08 PW using Hellerman and Rosenstein winds [*Hellermann and Rosenstein*, 1983]. Most of these early studies are based on quasisynoptic sections and are therefore unable to provide long-term statistics of the MHT.

Table 1. Previous Estimates and New Estimates of MOC Strength and MHT in the South Atlantic[a]

Latitude	Source	MOC (Sv)	MHT (PW)
45°S	*Saunders and King* [1995]	—	0.94
35°S	*Garzoli et al.* [2013]	18.10 ± 2.30	0.54 ± 0.14
35°S	*Garzoli and Baringer* [2007]	—	0.54 ± 0.11
35°S	This study (Argo and SSH)	20.66 ± 4.13	0.66 ± 0.21
34°S	*Dong et al.* [2014]	18.40 ± 2.39	0.53 ± 0.17
34°S	*Dong et al.* [2015]	19.45	0.49
30°S	*Baringer and Garzoli* [2007]	—	0.40
30°S	*Dong et al.* [2015]	20.62	0.70
30°S	*de las Heras and Schlitzer* [1999]	—	−0.23
30°S	*Fu* [1981]	—	0.8
30°S	*Ganachaud and Wunsch* [2003]	—	0.4
30°S	*McDonagh and King* [2005]	—	0.22 ± 0.08
30°S	This study (Argo and SSH)	23.36 ± 4.61	0.76 ± 0.22
24°S	*Bryden et al.* [2011]	21.5	0.40
25°S	*Dong et al.* [2015]	18.24	0.94
25°S	This study (Argo and SSH)	27.97 ± 2.83	0.92 ± 0.15
20°S	*Dong et al.* [2015]	17.24	1.22
20°S	This study (Argo and SSH)	17.10 ± 2.45	0.53 ± 0.16

[a]For Argo and SSH means and standard deviations are provided.

The availability of new observations in recent years has improved our understanding and led to more robust means. *Garzoli and Baringer* [2007] used 14 expandable bathythermograph (XBT) transects at a nominal latitude of 35°S from years 2002 to 2006 and reported a mean MHT of about 0.54 PW. Using an additional year of XBT observations near 35°S, *Dong et al.* [2009] obtained a mean MOC strength of 17.9 ± 2.2 Sv (1 Sv = 10^6 m^3 s^{-1}) between 2002 and 2007. Using more XBT transects (27 of them) and extended observations between years 2002 and 2011, *Garzoli et al.* [2013] analyzed meridional heat and salt fluxes in the South Atlantic and reported robust means of 18.1 Sv for the strength of the MOC and 0.54 PW for the MHT at 35°S.

Studies by *Dong et al.* [2009], *Meinen et al.* [2013], *Garzoli et al.* [2013], and *Dong et al.* [2015] discussed the variability of the MOC and its seasonality in the South Atlantic. *Dong et al.* [2009] observed that both the Ekman and geostrophic components are important in explaining the variability of the MOC, and found that its strength and MHT are strongly correlated at 35°S. The strength of the MOC estimated by *Meinen et al.* [2013] on the basis of a 20 month long time series in the western part of South Atlantic MOC Basin-wide Array (SAMBA) at 34.5°S is highly variable with values ranging from 3 to 39 Sv. *Meinen et al.* [2013] noted that two-thirds of the observed variability is due to the geostrophic component while the rest is due to the Ekman component. Looking at lower-frequency variability, *Dong et al.* [2014] used gridded Argo fields and model simulations between years 2004 and 2013 to analyze the seasonality of the MOC at 34°S and reported that the observations show a very different seasonal dependence than is detected in numerical models. Observations suggest that the Ekman and geostrophic contributions are equivalent but out of phase, while the models show very weak geostrophic seasonality that is in phase with the Ekman component. The weak seasonal cycle in the model geostrophic transport was attributed to strong baroclinicity below the mixed layer, not seen in the observations. Using altimetry-derived synthetic temperature fields between 20°S and 34.5°S, *Dong et al.* [2015] found that the seasonality is latitude-dependent and concluded that the contributions of the Ekman and geostrophic components depend on time and latitude.

In this study, a three-dimensional velocity field [*Schmid*, 2014] (Argo and SSH, hereinafter) based on Argo observations and sea surface heights from AVISO (Archiving, Validation, and Interpretation of Satellite Oceanographic data) [*Ducet et al.*, 2000], is used with gridded temperature and salinity fields from Argo floats to estimate the strength of the MOC and the MHT across four different latitudes (35°S, 30°S, 25°S, and 20°S) between March 2000 and May 2014. MOC strength and MHT from Argo and SSH are compared with the model-based estimates with the goal to improve our understanding of the variability and to analyze the contribution of boundary currents to the total transports.

This paper is organized as follows. The methodology and data sets are discussed in section 2. Section 3 discusses the results. Summary and conclusions are presented in section 4.

2. Data and Methods

Following a similar approach as *Willis* [2010], *Schmid* [2014] constructed a three-dimensional geostrophic velocity field using temperature, salinity, and float trajectories from Argo and sea surface heights (SSH) from AVISO. *Schmid* [2014] used this velocity field to understand the flow pattern and estimated meridional volume transport in the subtropical gyre. An updated version of this velocity field is used herein. The three-

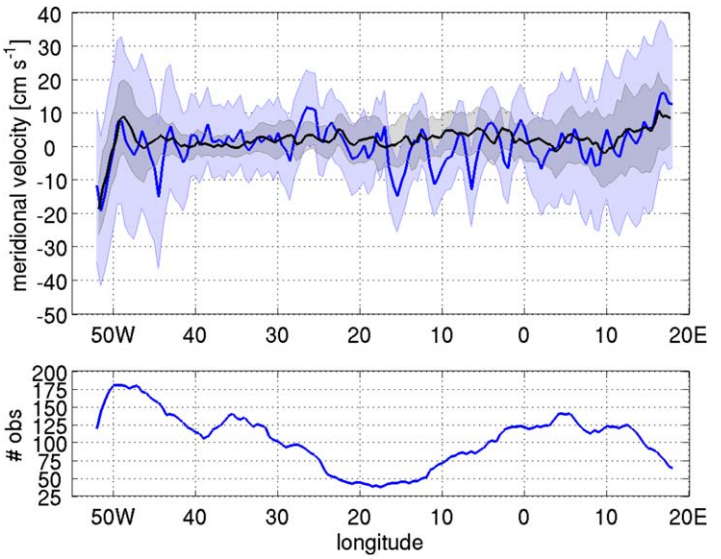

Figure 1. (top) Climatology of meridional velocity at 15 m from drifters (blue) and Argo and SSH (black) at 35°S. The shading shows the standard deviations. (bottom) Number of drifter days in a 1° × 1° box.

dimensional velocity field is derived following the methodology as *Schmid* [2014], with one improvement—daily rather than weekly fields from AVISO are used. A brief description of the methodology follows.

To compute the three-dimensional velocity field, profiles of temperature, and salinity are collected from Argo floats from March 2000 to May 2014 and subsurface float trajectories covering the period between 24 January 1990 and 4 January 2015 are also obtained. In addition, trajectories from nonprofiling floats going as far back as 1990 are used. SSH fields are obtained from AVISO. Both the profiles and trajectories, collected from the Argo Global Data Assembly Centers, go through a series of quality control procedures (a detailed description is available in *Schmid* [2014]).

Dynamic height fields are estimated from temperature and salinity profiles. Correlations between dynamic height and nearby daily SSH within 5° × 2° boxes with at least 10 data pairs are estimated on a 0.5° × 0.5° grid. These correlations are then used to construct synthetic dynamic height fields following *Schmid* [2014]. Monthly means of the synthetic dynamic height fields are used to get geostrophic velocity relative to a level of no motion at 1000 dbar. Absolute geostrophic velocity fields are obtained using velocities estimated from the subsurface float trajectories following the same method described in *Schmid* [2014]. This method includes extrapolation of the surface drift.

Since the methodology for deriving the velocity profiles does not take the bottom topography into account, the velocity profiles estimated from the synthetic heights can potentially extend beyond the bottom topography. Therefore, the profiles are shortened as needed on the basis of the sea floor elevation on a 2 min latitude/longitude grid [*Smith and Sandwell*, 1997].

The velocity from Argo and SSH at 35°S is first validated with observations from drifters collected in 1979 to March 2014 [*Lumpkin and Johnson*, 2013] (http://www.aoml.noaa.gov/phod/dac/dac_meanvel.php). For this comparison, velocities from Argo and SSH are vertically interpolated to 15 m, which is the depth for which the drifter velocity is valid. The annual mean climatology in the top panel of Figure 1 shows quite good agreement near the boundaries with the Brazil Current and the Brazil Return Current in the west and the Benguela Current in the east. For the Benguela Current, the mean difference is small. In the interior, the drifter velocity exhibits larger variability, which is most likely due to aliasing mesoscale variability that is not present in the Argo and SSH velocity. This is supported by the relative sparseness of drifter observations in the interior (Figure 1, bottom plot).

For selected monthly climatologies of the meridional velocity at 35°S (Figure 2), the situation is similar as for the annual mean climatology. For the Brazil Current, where the agreement of the annual climatology is good, a similar seasonality exists in both products (smaller velocity in August than in the other 3 months shown). Comparison at the other three latitudes studied herein also reveals generally good agreement with drifter velocities (not shown).

The hydrographic data from the profiling floats are also used to generate gridded fields of temperature and salinity in the upper 2000 dbar for use in the calculation of the MHT. Since temperature and salinity profiles from Argo typically end at about 2000 dbar, the velocity, temperature, and salinity fields are extended to the bottom using World Ocean Atlas 2013 [*Zweng et al.*, 2015; *Locarnini et al.*, 2013] 0.25° resolution gridded monthly climatology in the upper 1550 m and the annual gridded climatology below that depth. In

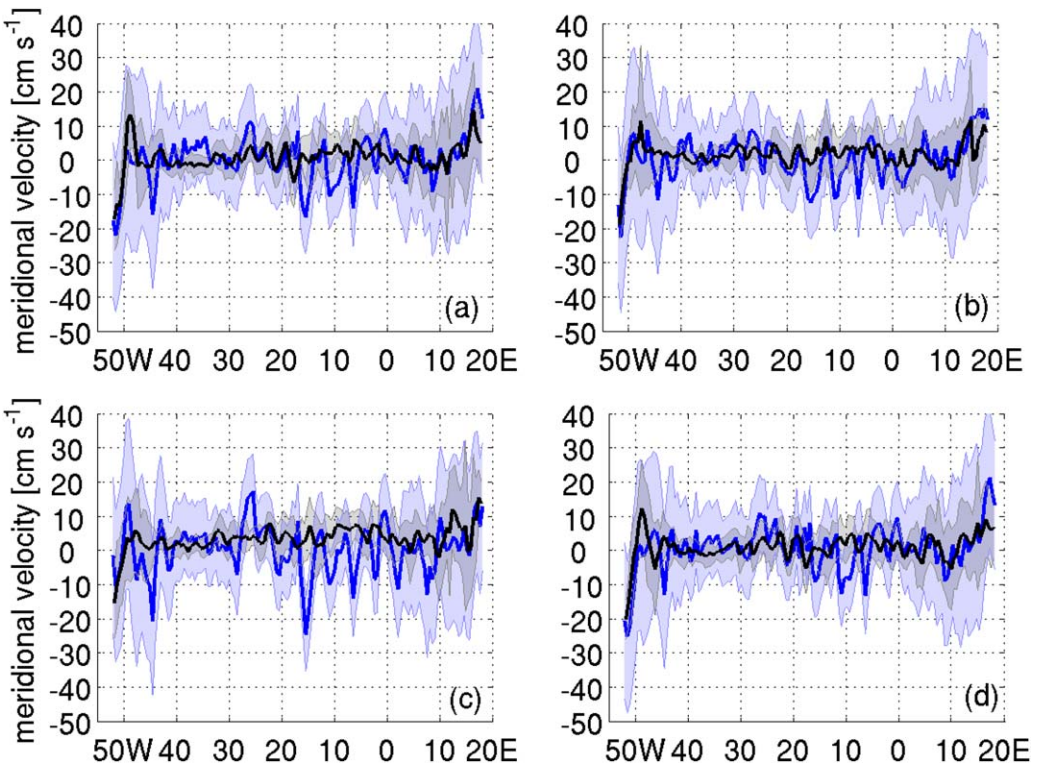

Figure 2. Monthly climatologies of meridional velocity from drifters (blue, at 15 m) and Argo and SSH (black) for the month of (a) January, (b) April, (c) August, and (d) December. The shading shows the standard deviations (for drifter velocities: only the standard deviation for the annual mean is available).

addition, climatologies from WOA are used at grid points and to the boundaries with insufficient hydrographic observations to generate robust temperature and salinity profiles through objective mapping for a given month and year. Density and heat capacity are derived from these fields.

A study of the Brazil Current (*Claudia Schmid and Sudip Majumder*, An observations and model-based analysis of the temporal variability of the Brazil Current, submitted to *Journal of Geophysical Research*, 2016) transports showed that the velocities from the Argo and SSH product underestimate the transports of this current at 35°S when compared with earlier studies. They found that a longitude-dependent barotropic adjustment of the meridional velocity to achieve a velocity of −0.04 to −0.08 m/s at 1000 dbar from 49.25°W to 51.75°W at 35°S yields transports that agree well with previous studies. This correction is applied at 35°S. For 20°S, 25°S, and 30°S they reported that no similar velocity correction is necessary. This velocity correction at 35°S is similar to *Garzoli and Baringer* [2007]'s and *Garzoli et al*. [2013]'s velocity adjustments. In those studies, about −0.04 m/s was added to the bottom velocities west of 40°W to approximate the barotropic southward flow in this region.

Finally, it is necessary to add the Ekman velocity to the geostrophic velocity. At 35°S, it is computed for multiple wind products (NCEP reanalysis 2 [*Kanamitsu et al*., 2002], CCMP-ATLAS [*Atlas et al*., 2011], and ERA-Interim [*Uppala et al*., 2005]) to study the impact of these different wind fields on the overall transports of the MOC. At all other latitudes, the velocity field is computed using NCEP reanalysis 2 (NCEP2) winds.

To estimate MOC and MHT at a given latitude, first the meridional volume, heat, and mass transports are calculated as a function of longitude, depth, and time. These transports are then adjusted to enforce a mass balance while taking the Bering Straits throughflow into account. The latter adjustment is based on the estimate of the salt flux of 27.6 kg s^{-1} through the Bering Straits [*Coachman and Aagaard*, 1988], following *Garzoli and Baringer* [2007], *Garzoli et al*. [2013], and *Dong et al*. [2015].

Next, MHT as a function of time is derived by integrating the adjusted heat transport zonally and vertically over the full length and depth of the section. To estimate MOC strength as a function of time, the adjusted

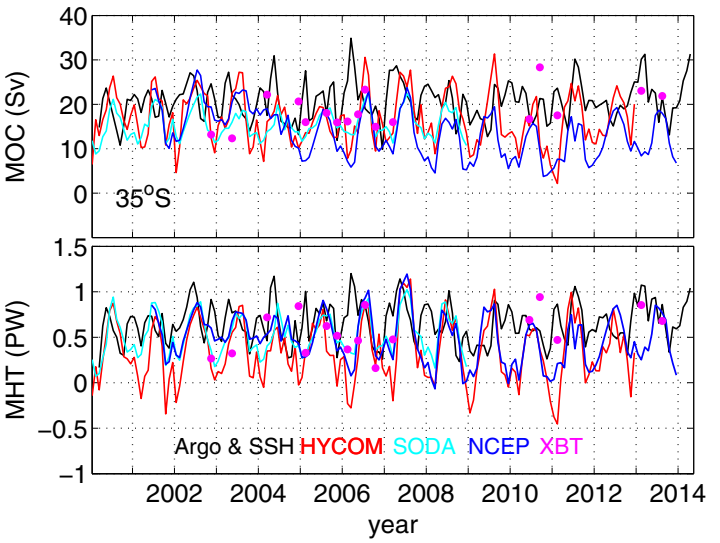

Figure 3. Strength of (top) MOC and (bottom) MHT at 35°S. Estimates from Argo and SSH (black), XBT lines between 33.5°S and 37°S (pink dots), NCEP/GODAS (blue), SODA (cyan) and HYCOM reanalysis (red).

volume transport is integrated zonally and then cumulatively from top to bottom. The MOC strength is the first maximum of this cumulative transport profile.

MOC strength and MHT from Argo and SSH are then analyzed in conjunction with the estimates from: (i) Expendable Bathythermograph (XBT) sections near 35°S and 30°S and (ii) results from three different global ocean reanalysis models with assimilation at four different latitudes (35°S, 30°S, 25°S, and 20°S).

The quality controlled XBT sections near 35°S from *Garzoli et al.* [2013] are used as independent observations for comparison with our estimates. *Garzoli et al.* [2013] obtained salinities for these profiles using a statistical T-S relationship. Because XBT profiles typically end at a depth of about 850 m, *Garzoli and Baringer* [2007] extended them to the bottom using climatological profiles from the World Ocean Atlas. They then calculate the geostrophic velocities from these profiles with a level of no motion at a potential density of 37.09 kg/m^3 (relative to 2000 m) and estimate the MOC strength as well as the MHT.

Of the three numerical models selected for comparison with the observations-based estimates, data from Hybrid Coordinate Ocean Model (HYCOM) is eddy resolving. HYCOM uses a Mercator grid patched to a curvilinear polar grid at high northern latitudes and has 32 vertical levels [*Chassignet et al.*, 2007]. The data obtained from Global 1/12° Reanalysis (GLBu0.08/expt-19.1) uses Navy Coupled Ocean Data Assimilation (NCODA) system for assimilation. Fields of temperature, salinity, and velocity from this model are collected between the years 2000 and 2012.

Temperature, salinity, and velocity fields between years 2000 and 2008, obtained from Simple Ocean Data Assimilation (SODA) [*Carton and Giese*, 2008), version 2.2.4, are coarse (0.5°) in the horizontal and have 40 vertical levels. Data from National Center for Environmental Prediction's Global Ocean Data Assimilation System (NCEP/GODAS) [*Kalnay et al.*, 1996] obtained between years 2000 and 2014, are available at every 1° in the horizontal and have 40 vertical levels.

Monthly averages of temperature, salinity, and velocity fields from these three models are used to estimate MOC strength and MHT. No adjustments for mass balance or Bering Straits throughflow are applied to the model transport estimates. All the transport estimates analyzed in the following are smoothed with a low-pass filter (a second order Butterworth filter).

3. Results

In the following sections, time series, mean values, and variability of MOC and MHT at different latitudes (35°S, 30°S, 25°S, and 20°S, Figures 3–6) are presented. The time series are smoothed to focus only on the seasonal and interannual variability. The estimates from HYCOM are governed by strong variability because of the high temporal and spatial resolution of this model. However, a large part of the variability has been filtered out.

3.1. Transports at 35°S

Mean MOC strength and MHT from Argo and SSH (derived following the method described in section 2) at 35°S are 20.66 Sv and 0.66 PW (Table 2). These numbers are a bit higher than the estimates from AX18 sections nominally at 35°S (18.46 Sv, 0.56 PW) as well as those from *Baringer and Garzoli* [2007], *Garzoli et al.*

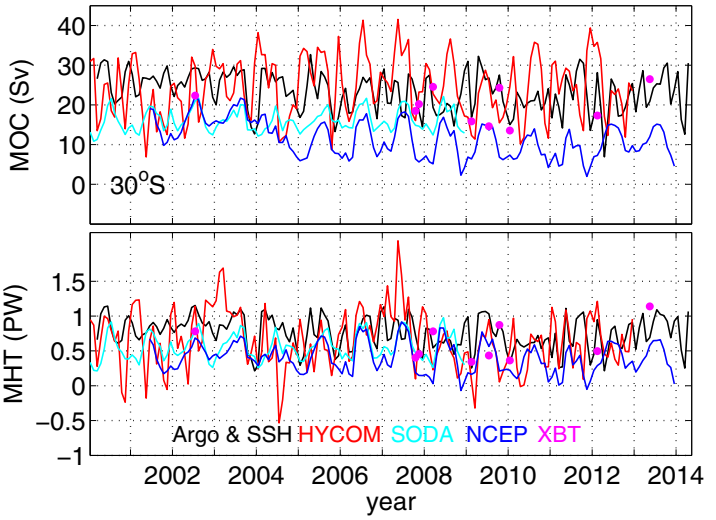

Figure 4. Strength of (top) MOC and (bottom) MHT at 30°S. Estimates from Argo and SSH (black), XBT lines between 28S and 32S (pink dots), NCEP/GODAS (blue), SODA (cyan) and HYCOM reanalysis (red).

[2013], and *Dong et al.* [2014] for 34°S (Table 1). The MHT is also higher than the value derived by *Dong et al.* [2015] but the agreement of the MOC strength is quite good. Mean MOC strength and MHT from Argo and SSH are higher than the estimates from HYCOM (16.67 Sv, 0.34 PW), SODA (15.49 Sv, 0.52 PW), and NCEP/GODAS (13.58 Sv, 0.49 PW). HYCOM has the lowest mean MHT because of the quite low or even negative values mainly in austral summer (Figure 3). During the season of high MHT, around the middle of the year, HYCOM has similar values for MHT to SODA. NCEP/GODAS exhibits a mean negative trend of about −0.65 Sv/year, while no trend can be detected in the other estimates. This trend gives rise to the low mean MOC strength from NCEP/GODAS because this model is very close to the other models in the early years of the time series and diverges from them gradually.

With respect to the temporal variability, one can see a strong annual cycle for MOC and MHT from the models with transport maxima in austral winter and minima in austral summer in most years. Annual cycles in the time series based on Argo and SSH have different phasing than those from models. Until about 2007, the maxima mostly occur 1–3 months earlier than in models. In the later years, the maxima of the MOC strength sometimes occurs in the same month as for HYCOM (e.g., 2009 and 2011) while it is absent in other years (e.g., 2010 and 2012).

3.2. Transports at 30°S

The average strengths of MOC and MHT from HYCOM and Argo and SSH at 30°S are similar, within 1 Sv and 0.1 PW of each other, respectively (Table 2). The mean MHT of 0.76 PW from Argo and SSH is very similar to the values reported by *Dong et al.* [2015] and *Fu* [1981], but it is larger than other previous estimates (Table 1). The strength of the MOC is somewhat larger than the one reported by *Dong et al.* [2015], but the difference is smaller than the standard deviation from the Argo and SSH estimate.

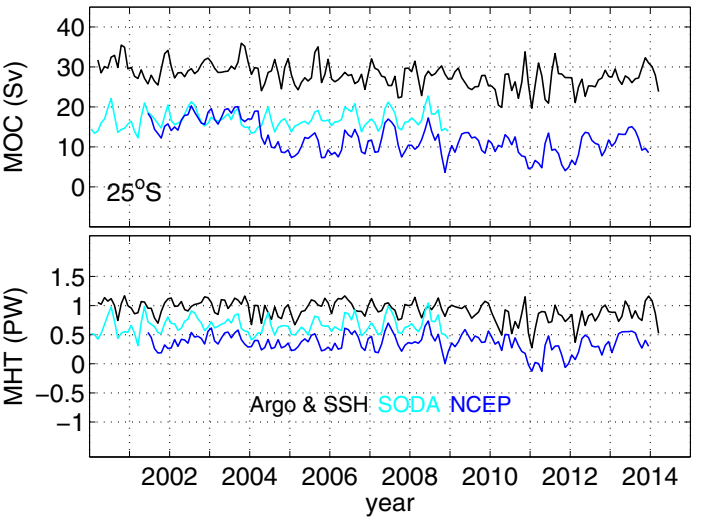

Figure 5. Strength of (top) MOC and (bottom) MHT at 25°S. Estimates from Argo and SSH (black), NCEP/GODAS (blue), and SODA (cyan). Results from HYCOM are not shown.

The mean MOC strength and MHT from Argo and SSH are also higher than the estimates from AX18 (19.78 Sv, 0.61 PW), but the difference is not very significant because it is only slightly larger than the standard deviation from Argo and SSH (Table 2). In contrast to that, the strength of the MOC from SODA and, even more so, NCEP/GODAS is much smaller than that from all observations as well as HYCOM. With respect to the MHT, SODA, and NCEP/GODAS also have

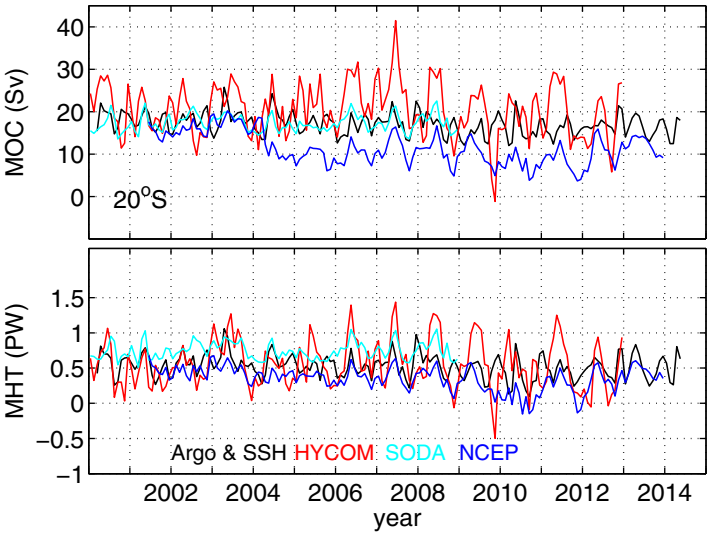

Figure 6. Strength of (top) MOC and (bottom) MHT at 20°S. Estimates from Argo and SSH (black), NCEP/GODAS (blue), SODA (cyan) and HYCOM reanalysis (red).

smaller values, but they stand out less. NCEP/GODAS shows about a 5 Sv decrease in the mean AMOC strength from 2004 onward (Figure 4). This decrease in the mean AMOC strength is not seen in the other estimates.

In most years, a strong annual cycle with maximum in June and minimum between November and January can be observed both in Argo and SSH and in two of the model estimates in Figure 4. HYCOM estimates, however, have two distinct maxima in June and January and minima in April and October in most years.

3.3. Transports at 25°S

The mean MOC strength and MHT from Argo and SSH are 27.97 Sv and 0.92 PW. These numbers are higher than the model estimates (Table 2 and Figure 5) and the values previously reported by *Bryden et al*. [2011] at 24°S (21.5 Sv and 0.4 PW) and *Dong et al*. [2015] (18.24 Sv, Table 1) at 25°S. Mean MHT from Argo and SSH, however, is similar to the estimate (0.94 PW) by *Dong et al*. [2015]. The relatively weak MOC strengths and MHTs in the models vary from ∼12 Sv (0.36 PW, NCEP/GODAS) to ∼16.79 Sv (0.66 PW, SODA).

Among the models NCEP/GODAS exhibits the weakest mean MOC strength. Even though the mean MOC strength in NCEP/GODAS is similar to SODA (16.79 Sv, Figure 5) in the beginning of the time series between 2001 and 2004, it decreases by ∼8 to 10 Sv in 2005 and stays lower thereafter bringing down the overall mean to 11.93 Sv (Table 2). Mean MHT from NCEP/GODAS does not show any decrease in 2005 as seen in the MOC strength.

Estimates from HYCOM are unrealistic at 25°S, therefore the results from this model are not shown (see Appendix A).

3.4. Transports at 20°S

Mean MOC strength and MHT from Argo and SSH are 17.10 Sv and 0.53 PW (Table 2) at 20°S. These values are similar (within the error bars) to the mean MOC strength from SODA and mean MHT from HYCOM. The

Table 2. Estimates of Mean and Standard Deviation of MOC Strength and MHT From Argo and SSH and Models

Latitude	Based on	Duration	MOC (Sv)	MHT (PW)
35°S	Argo and SSH	2000–2014	20.66 ± 4.13	0.66 ± 0.21
35°S	HYCOM	2000–2012	16.67 ± 5.57	0.34 ± 0.32
35°S	SODA	2000–2008	15.49 ± 3.08	0.52 ± 0.22
35°S	NCEP	2001–2013	13.58 ± 5.37	0.49 ± 0.26
35°S	AX18	2002–2013	18.46 ± 4.17	0.56 ± 0.23
30°S	Argo and SSH	2000–2014	23.36 ± 4.61	0.76 ± 0.22
30°S	HYCOM	2000–2012	24.37 ± 7.22	0.66 ± 0.38
30°S	SODA	2000–2008	16.09 ± 2.61	0.56 ± 0.18
30°S	NCEP/GODAS	2001–2013	11.56 ± 4.48	0.40 ± 0.21
30°S	AX18	2002–2013	19.78 ± 4.52	0.61 ± 0.27
25°S	Argo and SSH	2000–2014	27.97 ± 2.83	0.92 ± 0.15
25°S	SODA	2000–2008	16.79 ± 2.08	0.66 ± 0.14
25°S	NCEP/GODAS	2001–2013	11.93 ± 3.80	0.36 ± 0.15
20°S	Argo and SSH	2000–2014	17.10 ± 2.45	0.53 ± 0.16
20°S	HYCOM	2000–2012	20.49 ± 5.87	0.55 ± 0.33
20°S	SODA	2000–2008	17.33 ± 1.90	0.75 ± 0.11
20°S	NCEP/GODAS	2001–2013	11.43 ± 3.73	0.35 ± 0.16

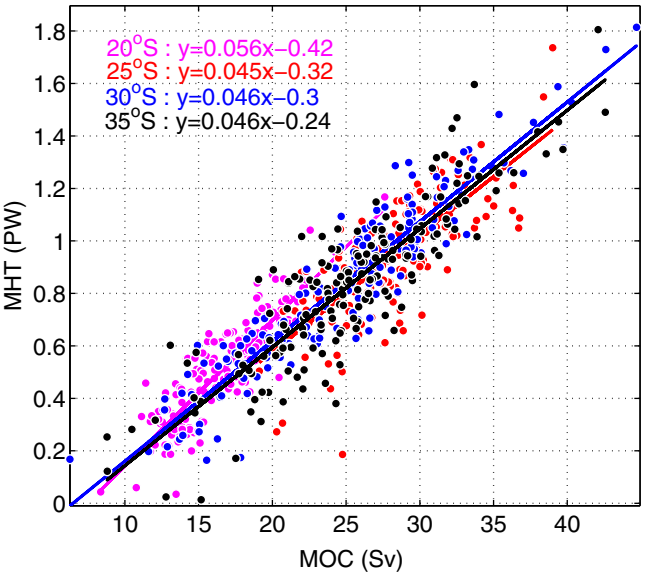

Figure 7. (top) Scatter plot of MOC strengths against MHTs from Argo and SSH for different latitudes: 20°S (magenta), 25°S (red), 30°S (blue) and 35°S (black). (bottom) Straight lines are the corresponding linear fits.

fact that there are fewer observational studies at this latitude, however, makes it difficult to present a similar comparison as shown for the other latitudes. The only observational study at 20°S by *Dong et al*. [2015] reported similar mean MOC strength (of 17.24 Sv) as Argo and SSH, but observed about 2.3 times higher mean MHT (Table 1) than the present study. The mean MHT from Argo and SSH is within the range shown in Figure 13 in *Garzoli and Baringer* [2007] and is within the error bars of the estimate by *Holfort and Siedler* [2001] with inverse modeling (also shown in the same figure).

Among all the estimates, NCEP/GODAS has the minimum MOC strength of 11.43 Sv and MHT of 0.35 PW. The mean MHT from NCEP/GODAS is similar to that from Argo and SSH within the standard deviation, but the strength of the MOC is about 5 Sv smaller. The strength of the MOC from NCEP/GODAS is comparable to the other estimates between 2001 and 2005, but weakens by ∼5 Sv from 2005 to 2006 and thereafter, maintains a mean MOC of about 10 Sv (Figure 6 and Table 2). This decrease in the strength of the MOC between 2005 and 2006 explains the relatively weak values observed in NCEP/GODAS.

Strong annual cycles can be observed in the model estimates, with maximum in April and minimum in October. However, observations show a weak semiannual cycle with maxima mostly in April and October. A detailed analysis of the seasonality is presented in section 3.6.

3.5. Correlation of MOC Strength and MHT

Using XBT sections, *Dong et al*. [2009] observed a strong correlation between the MOC strength and MHT at 35°S, and found that MHT changes about 0.064 PW for 1 Sv change in MOC strength at this latitude. A similar analysis at 35°S, 30°S, 25°S, and 20°S is shown in Figure 7 and Table 3. MOC strength and MHT from Argo and SSH (Figure 7) show strong correlations at all the latitudes. The corresponding change in MHT for 1 Sv change in MOC strength is about 0.046 ± 0.001 PW at 35°S, 0.046 ± 0.0007 PW at 30°S and 0.045 ± 0.005 PW at 25°S (Figure 7). More heat, about 0.056 ± 0.002 PW, is transferred for a 1 Sv change in MOC strength at 20°S. An important point to note from Figure 7 is that the MHT change for a 1 Sv MOC strength change (called slope, hereinafter) across all three southern most latitudes (35°S, 30°S, and 25°S) is about the same. In a previous study, *Dong et al*. [2015] reported latitude-dependent slopes of 0.040 PW/Sv, 0.022 PW/Sv, and 0.050 PW/Sv at 34.5°S, 30°S, and 25°S, respectively. Also, at 20°S, the corresponding slope found herein is about 0.02 PW/Sv larger than the result of 0.033 PW/Sv by *Dong et al*. [2015].

Table 3. Relationship Between MOC Strength and MHT

Latitude	Based on	Linear fit
35°S	Argo and SSH	$MHT = 0.046 \times MOC - 0.24$
35°S	SODA	$MHT = 0.068 \times MOC - 0.54$
35°S	HYCOM	$MHT = 0.044 \times MOC - 0.35$
35°S	NCEP/GODAS	$MHT = 0.045 \times MOC - 0.12$
30°S	Argo and SSH	$MHT = 0.046 \times MOC - 0.30$
30°S	SODA	$MHT = 0.068 \times MOC - 0.53$
30°S	HYCOM	$MHT = 0.030 \times MOC - 0.02$
30°S	NCEP/GODAS	$MHT = 0.041 \times MOC - 0.06$
25°S	Argo and SSH	$MHT = 0.045 \times MOC - 0.32$
25°S	SODA	$MHT = 0.064 \times MOC - 0.41$
25°S	NCEP/GODAS	$MHT = 0.028 \times MOC - 0.03$
20°S	Argo and SSH	$MHT = 0.056 \times MOC - 0.42$
20°S	SODA	$MHT = 0.059 \times MOC - 0.27$
20°S	HYCOM	$MHT = 0.046 \times MOC - 0.37$
20°S	NCEP/GODAS	$MHT = 0.033 \times MOC - 0.01$

The models also show strong correlations between MHT and MOC strength. Most of the models have similar slopes (about 0.04 PW/Sv) as Argo and SSH at 35°S and 30°S (Table 3). The

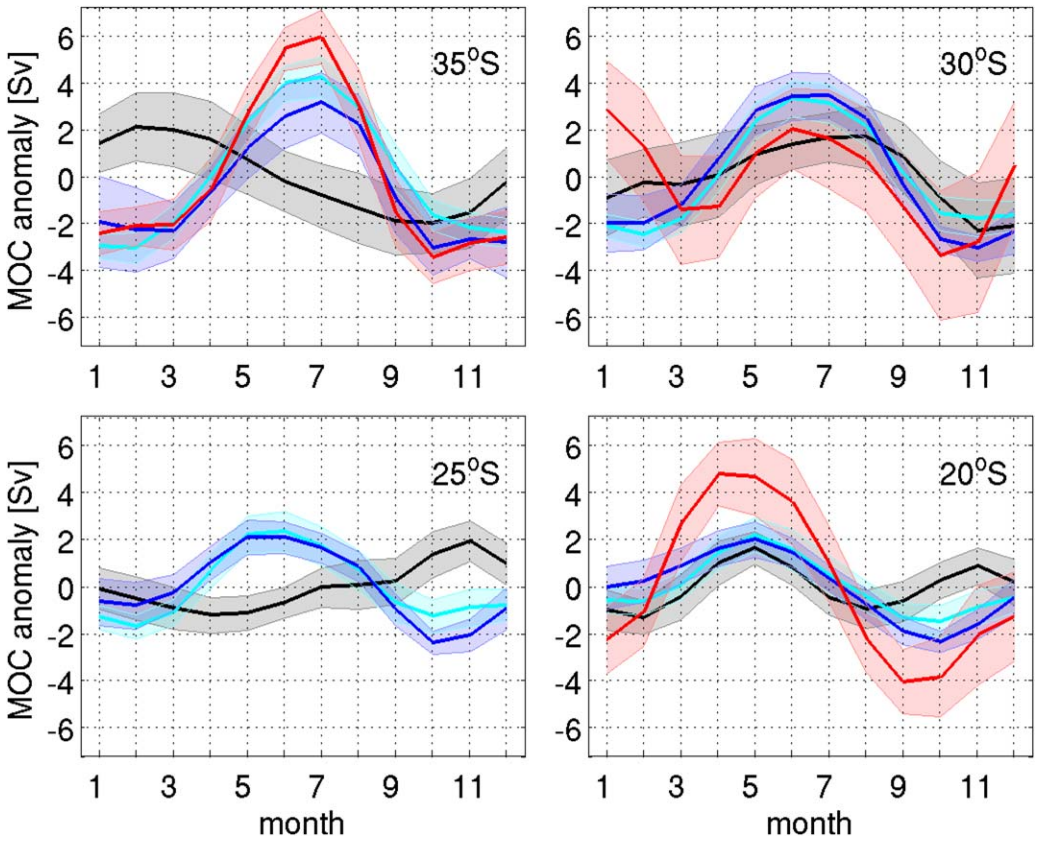

Figure 8. Monthly climatologies of anomalies of MOC strengths across 35°S, 30°S, 25°S, and 20°S from Argo and SSH (black), NCEP/GODAS (blue), SODA (cyan), and HYCOM (red). Shading indicates 95% confidence interval. Results from HYCOM are not shown for 25°S.

exception is SODA with a slope that is about 0.02 PW/Sv larger (0.068 PW/Sv) at these latitudes. At 25°S, the slopes for the models deviate significantly from those derived for Argo and SSH. At 20°S, the situation improves slightly, i.e., slopes from SODA and Argo and SSH are similar while those from NCEP/GODAS and HYCOM are lower.

At 35°S and 30°S, the slopes from the models are mostly close to those from Argo and SSH, with two exceptions: (1) SODA has relatively high values at the southern three latitudes and (2) HYCOM has a relatively small slope at 30°S. For SODA, the MOC strength is relatively low at these three latitudes (Figures 3–5) which can be attributed to relatively large Brazil Current transports (*Claudia Schmid and Sudip Majumder*, An observations and model-based analysis of the temporal variability of the Brazil Current, submitted manuscript, 2016). For HYCOM, the reason is a relatively large scatter of the strength of MOC and the MHT, which can be attributed to barotropic currents that have some impact at 30°S (these currents are strongest at 25°S where HYCOM fields cannot be used to derive the integrated transports, Appendix A). At 25°S and 20°S, the slopes for NCEP/GODAS are smaller than the slope for Argo and SSH. However, the scatter plots (not shown) indicate that these slopes are not robust. An indication of this can be seen in the time series plots (Figures 5 and 6) in which the strength of the MOC changes quite strongly around 2004 while the MHT does not reveal a corresponding change (section 3).

3.6. Seasonality

Time series of the strength of MOC and MHT show seasonal variability both in Argo and SSH and model-based estimates. However, a more detailed analysis is needed to achieve a better understanding of the seasonality of these transports. This is done by deriving a monthly climatology of the anomalies of MOC strengths at different latitudes (Figure 8).

At 35°S, the anomalies of the strength of MOC from Argo and SSH reveal a clear annual cycle with maximum in austral summer to fall and minimum in austral spring. In contrast to this, the maxima in the models occur

in a later season (austral winter) while the timing of the minima in austral spring to summer overlaps with that from Argo and SSH. When taking the Argo and SSH time series into account the largest maxima occur in austral fall in nine of the years while only three (two) are found in austral summer (winter). When taking all maxima into account, one finds 10 peaks in austral fall and seven in austral summer. Such interannual variations are not present in the models. A plausible reason for the interannual variability is the complex nature of the circulation at 35°S, which is greatly influenced by the Brazil and Benguela Currents as well as by the Agulhas Rings. It was shown, for example, that the transport variations of the Brazil Current depend strongly on the latitude (e.g., *Claudia Schmid and Sudip Majumder*, An observations and model-based analysis of the temporal variability of the Brazil Current, submitted manuscript, 2016) [*Garzoli et al*., 2013]. Agulhas Rings are likely to only have an impact south of 30°S, due to the fact that they typically travel predominantly westward once they left the Cape Basin [*Richardson*, 2007; *Gordon and Haxby*, 1990].

At 30°S, the agreement between Argo and SSH and the models is much better with maxima in austral winter and minima in austral summer (Figure 8). The exception is HYCOM, which exhibits a semiannual cycle with maxima (minima) in austral summer and winter (austral spring and fall) that can also be seen in the time series plot (Figure 4). In terms of interannual variability, the Argo and SSH time series also reveals high values in austral summer in 6 years, but these are not significant with respect to the mean annual cycle.

The annual cycle at 25°S from SODA and NCEP/GODAS is about half as large as at 30°S and 35°S (Figure 8), while the amplitude reduction for Argo and SSH is smaller. In addition, it is noted that the standard errors are about half as large at 25°S as at the other two latitudes, which is indicative of a difference in regimes. For the NCEP/GODAS and SODA models, the timing of the maxima and minima at 25°S is similar to the one encountered at the other two latitudes. For Argo and SSH, the phase shift seen between 35°S and 30°S (maximum in austral summer/fall versus austral winter) continues, with the maximum found in austral spring at 25°S. Since HYCOM estimates are unrealistic at this latitude its seasonality is not discussed here (see Appendix A).

Argo and SSH at 20°S reveals a weak indication of a semiannual cycle with a strong maximum in austral fall and a weak maximum in austral spring. The minima can be seen in austral winter and summer. Model-based anomalies, on the other hand, reveal only annual cycles with maxima in austral fall and minima in austral spring. A discrepancy in seasonality between the observations and models was also seen in the North Atlantic at 41°N by *Mielke et al*. [2013]. They reported a 180 degrees phase difference between the annual cycles from simulations from a NCEP-forced model and observations.

Dong et al. [2015] presented a seasonal analysis based on a mean annual cycle from which the annual mean was subtracted for the latitudes 34.5°S, 30°S, 25°S, and 20°S. They found distinct annual cycles at 34.5°S, 30°S, and 20°S. With the exception of 25°S, the amplitudes reported by *Dong et al*. [2015] are larger by up to a factor of two. When using their method, we get similar amplitudes at all latitudes except 25°S (not shown). This is due to the difference in methodology between *Dong et al*. [2015] and this study, which also leads to small discrepancies in the seasonality. The timing of the minima at 35°S and 30°S derived herein agree quite well with *Dong et al*. [2015], while the timing of the maxima is 2–3 months off. At 25°S, a clear annual cycle was detected herein, while the result by *Dong et al*. [2015] was inconclusive due to a very small amplitude of the signal. At 20°S, the timing of the maximum detected by *Dong et al*. [2015] agrees well with the one found herein (austral fall), and both studies found a minimum a few months later. It remains to be seen if a significant semiannual cycle exists at this latitude.

Five key points are noted from Figure 8: (i) anomalies of MOC strength from Argo and SSH have strong seasonal signals at all four latitudes; (ii) the standard errors at 35°S and 30°S are about twice as large as at 25°S and 20°S; (iii) the timing of the maxima and minima changes from latitude to latitude; (iv) a weak sign for a semiannual cycle is found at 20°S; (v) MOC anomalies from Argo and SSH and models do not agree well on the phase and the amplitude of the seasonal cycle. Based on these key findings, it appears that different regimes govern the circulation at the northern and southern two latitudes studied herein. Possible contributing factors to the differences are: (1) winds closer to the equator (i.e., north of 25°S) have a different pattern than the subtropical winds further south. As a consequence of this the Ekman component, which is an important contributor to the seasonality of the MOC [*Dong et al*., 2014], is different in these two regimes; (2) the area south of about 25°S is dominated by the subtropical gyre, while strong zonal alternating subsurface currents are present in the north; (3) large variability near the boundaries, in the Brazil and Benguela Current regimes, is stronger in the southern regions of the study area. This region is also strongly affected by Agulhas

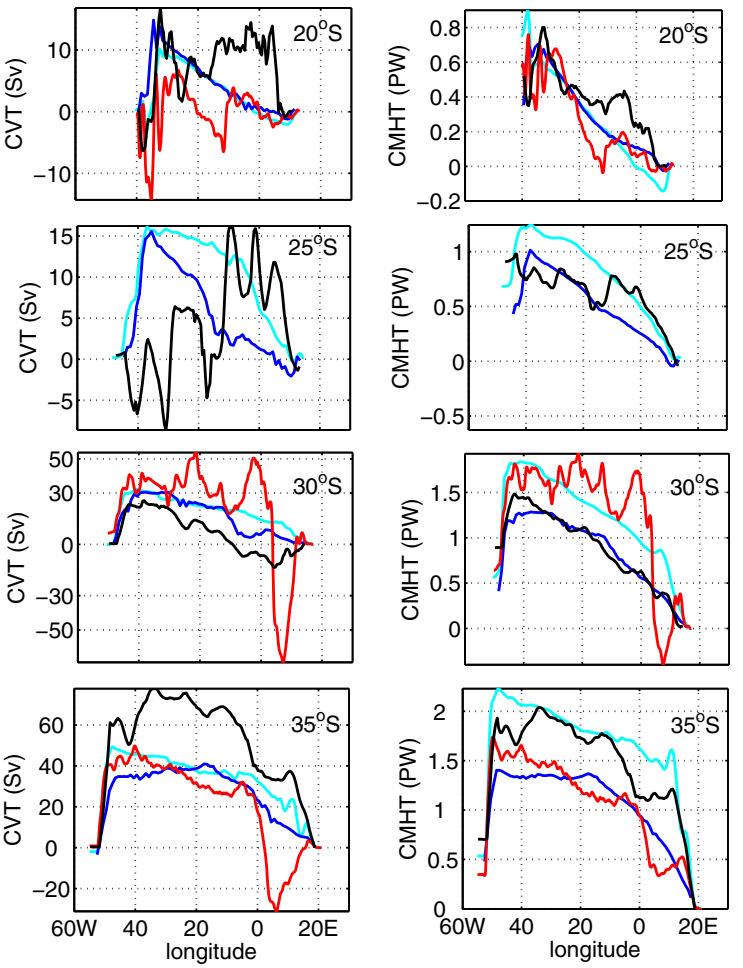

Figure 9. Climatologies of cumulative volume transport (CVT) and basin integrated meridional heat transport (CMHT) across 20°S, 25°S, 30°S, and 35°S from Argo and SSH and models. Both transports were integrated from top to bottom. Estimates from HYCOM are not shown for 25°S.

Rings. It seems likely that all of these effects have an impact on the latitude dependence of the seasonality. Also, because the representation of these characteristics within the models depends on their resolution, they are likely to give rise to the differences between the models.

3.7. Longitudinal Dependence

To understand the distribution of meridional volume and heat transports at different longitudes, climatologies of cumulative basin-integrated volume transport and MHT (hereafter, CVT and CMHT) are estimated for Argo and SSH and models at different latitudes. Figure 9 shows CVT and CMHT, cumulatively integrated from east to west, for 20°S, 25°S, 30°S, and 35°S. The basin integrated volume transport is small due to the requirement of a mass balance adjusted by the Bering Straits throughflow (see section 2). Therefore, CVT from Argo and SSH at the westernmost longitude is negligible.

CVT from SODA and NCEP/GODAS has a similar distribution at all the latitudes (first column, Figure 9). At 30°S, CVT from Argo and SSH has similar variability as the estimates from these two models and also at 20°S and 35°S, at the western boundary, CVT from Argo and SSH is similarly distributed. However, Argo and SSH suggests stronger northward transport at the eastern boundary at 20°S, 25°S, and 35°S, as well as stronger northward transport in the interior at 35°S than SODA and NCEP/GODAS.

Even though CMHT from SODA and NCEP/GODAS have similar patterns, SODA exhibits higher values at 25°S, 30°S, and 35°S (second column, Figure 9). CMHT from Argo and SSH also shows similar distribution as these two models, and has values in between the estimates from SODA and NCEP/GODAS.

Since HYCOM is highly resolved both temporally and spatially, CVT and CMHT from this model exhibit maximum variability, with strong southward transports at the eastern boundary across 30°S and 35°S (Figure 9). Results from HYCOM at 25°S are not presented, because the climatology of meridional velocity from HYCOM reveals unrealistic strong barotropic components (see Appendix A).

3.8. Sectional Transports

To investigate the relative contribution of boundary currents and the interior to the total transport, meridional volume transport in the upper branch of MOC and meridional heat transport are estimated for three different sections: the eastern boundary (east of Greenwich Meridian), the western boundary (west of 48°W), and the interior (48°W to Greenwich Meridian). The acronyms UVT and HT are hereinafter used for sectional meridional volume transport at the upper branch of MOC and sectional meridional heat transport. The

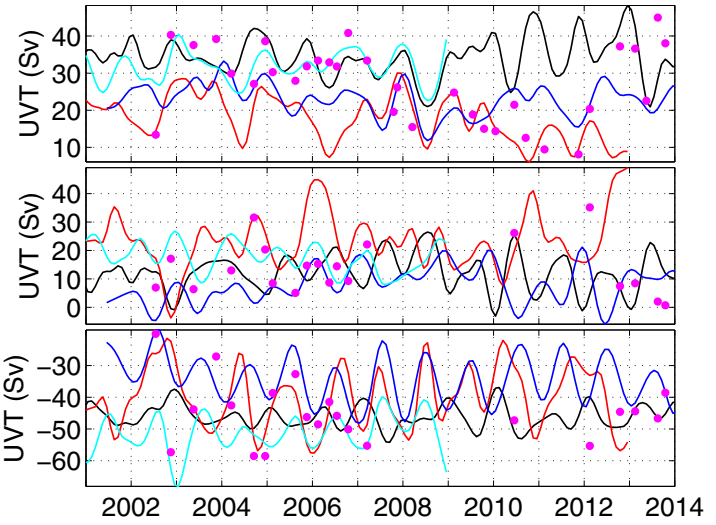

Figure 10. (top) Time series of the volume transport in the upper branch of the MOC at the eastern boundary (east of Greenwich Meridian) from Argo and SSH (black), AX18 (pink dots), NCEP/GODAS (solid blue), SODA (cyan) and HYCOM reanalysis (red). (middle) Same as top in the interior (48°W to the Greenwich Meridian). (bottom) Same as top at the western boundary (west of 48°W).

resulting smoothed time series for 35°S are shown in Figures 10 and 11, and the mean values are presented in Table 4.

Average contribution to UVT at the eastern boundary from Argo and SSH (33.65 Sv) is similar as SODA (32.13 Sv), but stronger than the mean values from NCEP/GODAS and HYCOM (top plot, Figure 11 and Table 4). Among all the estimates, HYCOM is the lowest with about 18 Sv. At the beginning (2000–2006) and towards the end (beyond 2013) of the time series, the transports from AX18 are similar to those from Argo and SSH and SODA, while they are weaker in 2007 to 2012. With respect to the HT at the eastern boundary, HYCOM, NCEP, and Argo and SSH show about the same mean HT (≈ 1.00 PW), while HT from SODA (1.61 PW) is the strongest.

Average UVT in the interior from Argo and SSH (12.72 Sv) is about half way in-between the estimates from NCEP/GODAS (7.95 Sv) and SODA (17.48 Sv). UVT from HYCOM exhibits maximum variability, with a mean two times stronger than that from ARGO and SSH (Figure 10). Even though UVT has different distribution in the models and in the observations, average HTs are similar (middle plot, Figure 11 and Table 4). Mean HT in the models and observations from Argo and SSH and AX18 varies between 0.45 PW (NCEP/GODAS) and 0.67 PW (HYCOM) in the interior.

Southward transport at the western boundary at 35°S is dominated by the Brazil Current. UVT from Argo and SSH reveals a mean southward transport of 46.07 Sv, comparable to the estimates from HYCOM (39.79 Sv) and SODA (51.68 Sv), but about 12 Sv stronger than the mean from NCEP/GODAS (Table 4, bottom plot, Figure 11). Southward mean HT from Argo and SSH is 1.02 PW, lies in between HYCOM (1.27 PW) and SODA (1.70 PW), while NCEP/GODAS has the weakest HT at the western boundary (0.89 PW).

Table 4. Estimates of Mean and Standard Deviation of the Volume and Heat Transports (UVT and HT) at the Boundaries and in the Interior

Based on	UVT (Sv)	HT (PW)
Eastern boundary		
Argo and SSH	33.65 ± 8.36	1.03 ± 0.18
HYCOM	18.42 ± 6.31	0.94 ± 0.21
SODA	32.13 ± 4.14	1.61 ± 0.11
NCEP	22.94 ± 4.28	0.93 ± 0.12
AX18	31.83 ± 8.04	1.25 ± 0.25
Interior		
Argo and SSH	12.73 ± 12.34	0.61 ± 0.45
HYCOM	22.51 ± 10.11	0.67 ± 0.33
SODA	17.48 ± 5.04	0.61 ± 0.15
NCEP	7.95 ± 6.17	0.45 ± 0.17
AX18	13.18 ± 10.08	0.45 ± 0.32
Western boundary		
Argo and SSH	−46.07 ± 6.66	−1.02 ± 0.43
HYCOM	−39.79 ± 9.57	−1.27 ± 0.33
SODA	−51.68 ± 5.70	−1.70 ± 0.20
NCEP	−34.24 ± 7.20	−0.89 ± 0.26
AX18	−44.72 ± 14.96	−1.11 ± 0.47

Both UVT and HT in the interior and at the eastern boundary are northwards. Transport at the eastern boundary, in general, is smaller than in the interior. For Argo and SSH, UVT and HT at the eastern boundary are about 60% and 40% smaller than the interior. UVT and HT from SODA (50% and 60%), NCEP (65% and 50%), and AX18 (60% and 60%) too have similar smaller values at the eastern boundary. On the contrary, UVT from HYCOM at the eastern boundary is about 20% larger; however, HT from HYCOM is about 30% smaller than in the interior.

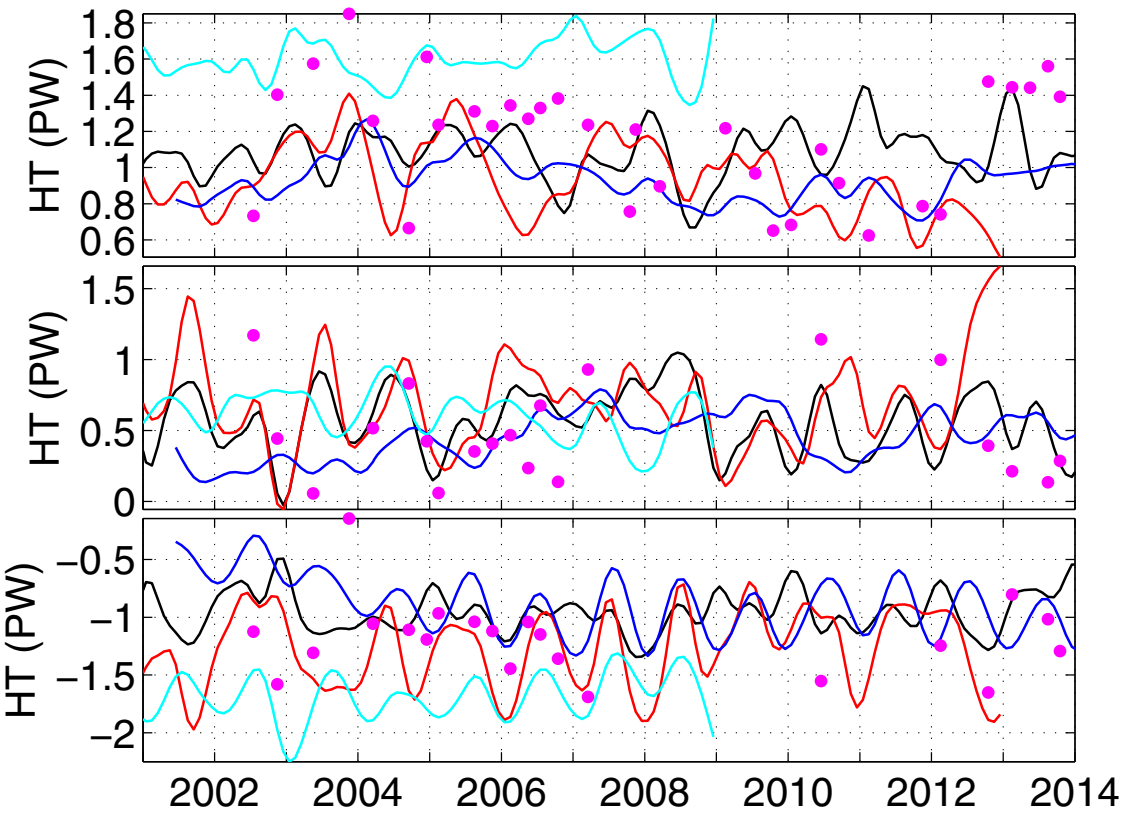

Figure 11. (top) Time series of the meridional heat transport at the eastern boundary (east of Greenwich Meridian) from Argo and SSH (black), AX18 (pink dots), NCEP/GODAS (solid blue), SODA (cyan), and HYCOM reanalysis (red). (middle) Same as top for the interior (48°W to the Greenwich Meridian). (bottom) Same as top for the western boundary (west of 48°W).

Adding up the interior and western boundary transports reduces the difference between the various estimates significantly. Although all the estimates show a pronounced annual cycle, the models and observations indicate different phasing.

3.9. Geostrophic and Ekman Contributions to the MOC and MHT

The Ekman transport is derived based on NCEP2 wind fields at 35°S. The geostrophic and Ekman contributions to the MOC and MHT are presented in Figures 12 and 13. The geostrophic contribution to the MOC (MHT) is 24 Sv (0.8 PW) which is about six (eight) times stronger than those due to the Ekman transport. This result does not change significantly if ERA-Interim wind fields are used (Figure 14). The CCMP-ATLAS wind fields yield about 0.2 PW and 1.5 Sv weaker transport than NCEP2.

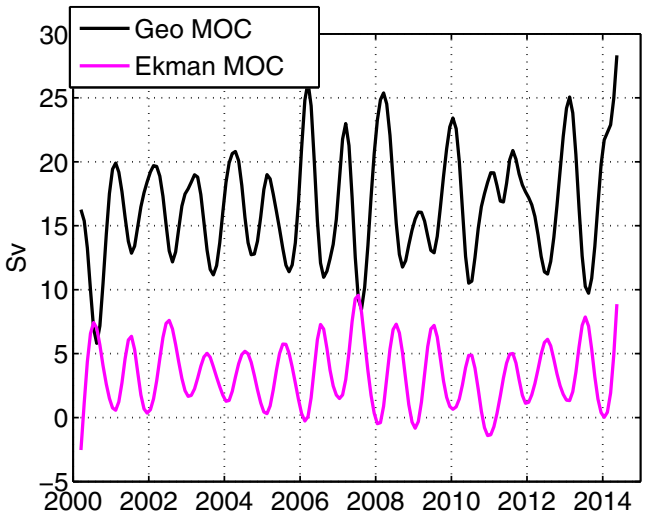

Figure 12. Time series of geostrophic (black) and wind-driven (pink) contributions to the MOC strength for Argo and SSH.

4. Summary and Discussions

An approximately 15 year long time series of transports was derived from observations (Argo and SSH) to understand the variability of the MOC in conjunction with corresponding estimates

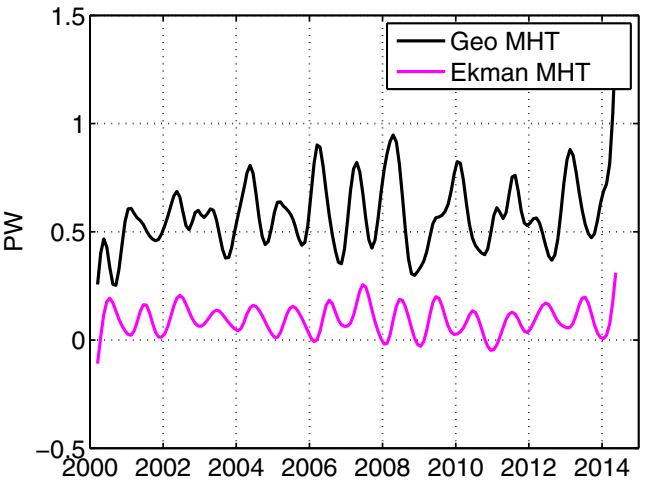

Figure 13. Time series of geostrophic (black) and wind-driven (pink) contributions to MHT for Argo and SSH.

from three different models at four different latitudes (20°S, 25°S, 30°S, and 35°S) in the South Atlantic. This joint analysis explains how model-based estimates are similar or different than the observations with respect to the mean strength, seasonality, and relative distribution of volume and heat transports, both spatially and temporally.

The majority of the estimates presented here are consistent with previous studies in the South Atlantic. For example, at 35°S, the mean MOC strength and MHT (about 20 Sv and 0.6) from Argo and SSH are close to the values (18 Sv and 0.5 PW) reported by *Garzoli et al.* [2013]. The estimates (23 Sv, 0.7 PW) at 30°S are similar to the estimates (21 Sv, 0.7 PW) by *Dong et al.* [2015]. Average MOC (28 Sv) at 25°S in this study is higher than that (18 Sv) observed by *Dong et al.* [2015]; however, MHT estimates are about the same (0.9 PW) at this latitude.

The methodology used here is similar to that of *Hobbs and Willis* [2012] but different than *Dong et al.* [2015]. *Hobbs and Willis* [2012] used Argo observations and SSH fields to estimate dynamic height and transports across 41°N in the North Atlantic between years 2002 and 2010, whereas *Dong et al.* [2015] used gridded temperature and SSH to generate synthetic temperature profiles and thereby salinity profiles using a historical T/S relationship to obtain MOC and MHT. One of the limitations of *Dong et al.* [2015] is the time dependence of the T/S relationship. Since this relationship may vary with time, *Dong et al.* [2015]'s methodology may not be suitable for monitoring long-term climate trends. Because this study uses temperature and salinity profiles directly from the floats, the methodology used here is suitable for predicting long-term climate trends.

Comparison of the results from observations (Argo and SSH) and models reveals that the Argo and SSH-based estimates are slightly higher than that from the models and have different phasing in seasonality. While the models mostly show annual cycles at all the four latitudes, Argo and SSH exhibit semiannual cycles at 20°S. Seasonality also differs in the models. Among the three models, HYCOM has the finest temporal as well as spatial resolution, therefore exhibiting maximum variability. SODA and NCEP/GODAS have the same phasing in seasonality and about the same amplitude. Even though HYCOM has the same annual cycles as SODA and NCEP/GODAS at 35°S and 20°S, the amplitude is relatively higher. The estimates from the models not only differ in mean strengths and seasonality but the MOC strengths at the boundaries and in the interior vary greatly in different models.

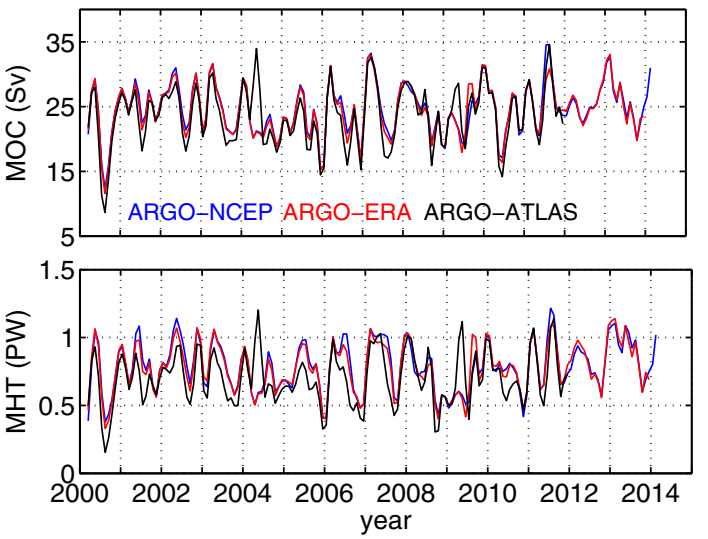

Figure 14. (top) Time series of MHT using the Argo and SSH in combination with three different wind products at 35°S. (bottom) Corresponding time series of MOC strengths. The wind products are NCEP2, ERA-Interim, and CCMP-ATLAS.

Not only the mean strength and seasonality, the models show different distribution of MOC at the boundaries and in the interior. Relatively smoothed SODA

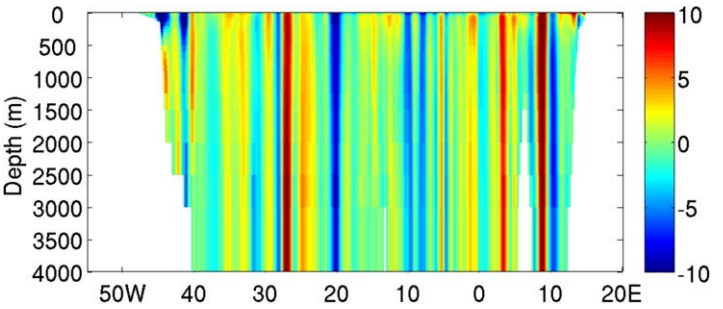

Figure 15. Climatology of meridional velocity (cm/s) from HYCOM at 25°S.

and NCEP/GODAS have some similarity with Argo and SSH in the longitudinal variability of MOC. However, strong eddy-like features are seen in the HYCOM estimates, especially at the eastern boundary. In spite of the dissimilarities, both Argo and SSH and model-based estimates show high correlations between MOC and MHT at all four latitudes.

Using XBT observations at 34.5°S, *Dong et al*. [2009] found a strong correlation between MOC strength and MHT. Extending their analysis for three other latitudes (20°S, 25°S, 30°S) and at 34.5°S, using sea surface height anomalies and gridded observations, *Dong et al*. [2015] found that the relationship between MOC strength and MHT varies with latitude and showed that 1 Sv change in MOC causes about 0.033 PW, 0.05 PW, 0.022 PW, and 0.04 PW change in MHT at 20°S, 25°S, 30°S, and 34.5°S, respectively. This study too finds strong correlations between MOC and MHT at all latitudes. However, the characteristics found herein are different. At 25°S, 30°S, and 35°S, 1 Sv change in MOC results in a MHT change of about 0.046 PW, whereas at 20°S a change of 0.056 PW is observed for 1 Sv change in MOC. Models also show good correlations at each latitude, but their specific linear fits deviate from those based on Argo and SSH to varying degrees.

An analysis of the annual cycle in the time series from Argo and SSH revealed differences between the four latitudes studied herein. The main differences are: there are changes in the phasing and amplitude from latitude to latitude; the size of the standard error is about half as large at 20°S and 25°S when compared with 30°S and 35°S; and a weak semiannual cycle is found at 20°S but not at any of the other latitudes. Models also reveal a change from the standard error found in Argo and SSH, and the phasing at 20°S is different from that found at the other latitudes.

The latitude-dependence of the annual cycle, as well as the relationship between the MOC strength and MHT, indicate the possibility of a regime change near 25°S to 20°S. In many ways, the regions north of 20°S and south of 25°S are different. The wind pattern and the circulation to the north of 20°S are dominated by the equatorial dynamics, whereas the southern part of this latitude band (20°S to 25°S) is governed by the subtropical gyre. In addition, the circulation in the southern latitudes, in general, is more complex due to its proximity to the Agulhas region and it being a region where the Brazil Current varies quite strongly (e.g., *Claudia Schmid and Sudip Majumder*, An observations and model-based analysis of the temporal variability of the Brazil Current, submitted manuscript, 2016) [*Garzoli et al*., 2013]. The former gives rise to variations of the Benguela Current and has an impact due to the shedding of Agulhas Rings, which typically stay south of 30°S [*Richardson*, 2007; *Gordon and Haxby*, 1990].

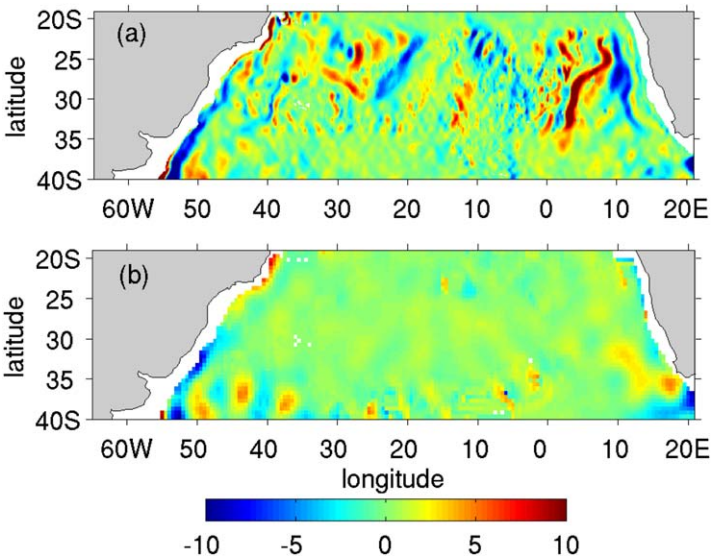

Figure 16. (a) Climatology of meridional velocity (cm/s) from HYCOM at 900 m. (b) Climatology of meridional velocity (cm/s) from Argo and SSH at 900 m.

The analysis presented in this study highlights the important

differences between observations (Argo and SSH based) and models, such as the difference in seasonality and the difference in sectional transports at the boundaries and in the interior. The results presented here can be used to validate and improve model simulations in the South Atlantic. Although a 15 year long time series is adequate to explain seasonal/annual cycles, extended observational surveys are required to understand decadal variability.

Appendix A: Why HYCOM Results Are Not Used at 25°S

Meridional velocity fields from HYCOM reveal strong and unrealistic bands with barotropic flow in the interior and at the eastern boundary (Figure 15). Such bands are not present in any of the other models or in Argo and SSH. This can be seen in Figure 16 which shows the climatology of the meridional velocity at 900 m from Argo and SSH and HYCOM. The map for HYCOM reveals many strong currents around 25°S while no such currents exist in the Argo and SSH map. Near the eastern boundary, these currents extend to 30°S, which is reflected in the cumulative volume transport shown in Figure 9 (third row, first column). Because the MOC strength and MHT at this latitude are comparable to the others the results for 30°S are included in this study.

Acknowledgments

This paper was funded by the Climate Observation Division, Climate Program Office, Climate Monitoring Program, National Oceanic and Atmospheric Administration, U.S. Department of Commerce and the Atlantic Oceanographic and Meteorological Laboratory of the National Oceanic and Atmospheric Administration. This research was also carried out in part under the auspices of the Cooperative Institute for Marine and Atmospheric Studies (CIMAS), a cooperative institute of the University of Miami and the National Oceanic and Atmospheric Administration (NOAA), cooperative agreement NA10OAR432013. The authors would like to thank the researchers and technicians involved in the Argo project for their contributions to generating a high-quality global sub-surface data set. The authors would also like to thank Dr. Elizabeth Johns, Dr. Marlos Goes, and Dr. Will Hobbs for their useful suggestions and comments. Argo data were obtained from the Global Data Assembly Centre (Argo GDAC, http://dx.doi.org/10.12770/71b7b0ed-1e3a-4ebc-8e3b-b5b363112f2a. Altimeter products were produced by Ssalto/Duacs and distributed by AVISO, with support from *Cnes* (http://www.aviso.altimetry.fr/ducas/). Funding for the development of HYCOM has been provided by the National Ocean Partnership Program and the Office of Naval Research. Data assimilative products using HYCOM are funded by the U.S. Navy. Computer time was made available by the DOD High performance Computing Modernization Program. The output is publicly available at http://hycom.org. NCEP reanalysis data (provided by NOAA/OAR/ESRL PSD, Boulder, Colorado, USA) were obtained from http://www.esrl.noaa.gov/psd/.

References

Atlas, R., R. N. Hoffman, J. Ardizzone, S. M. Leidner, J. C. Jusem, D. Smith, and D. Gombos (2011), A cross-calibrated, multi-platform ocean surface wind velocity product for meteorological and oceanographic applications, *Bull. Am. Meteorol. Soc.*, *92*(2), 157–174, doi:10.1175/2010BAMS2946.1.

Baringer, M., and S. Garzoli (2007), Meridional heat transport determined with expandable bathythermograph. Part 1: Error estimates from model and hydrographic data, *Deep Sea Res., Part I*, *54*, 1390–1401.

Broecker, W. S. (1997), Thermohaline circulation, the Achilles' heel of our climate system: Will man-made CO_2 upset the current balance?, *Science*, *278*, 1582–1588, doi:10.1126/science.278.5343.1582.

Bryden, L. B., B. A. King, and G. D. McCarthy (2011), South Atlantic overturning circulation at 24°S, *J. Mar. Res.*, *69*, 38–55.

Carton, J. A., and B. Giese (2008), A reanalysis of ocean climate using simple ocean data assimilation, *Mon. Weather Rev.*, *136*, 2999–3017.

Chassignet, E. P., H. Hurlburt, O. Smedstad, G. Halliwell, P. Hogan, A. Wallcraft, R. Baraille, and R. Bleck (2007), The hycom (HYbrid Coordinate Ocean Model) data assimilative system, *J. Mar. Res.*, *65*, 60–83.

Chidichimo, M. P., T. Kanzow, S. A. Cunningham, W. E. Johns, and J. Marotzke (2010), The contribution of eastern-boundary density variations to the Atlantic meridional overturning circulation at 26.5°N, *Ocean Sci.*, *6*, 475–490.

Coachman, L. K., and K. Aagaard (1988), Transports through Bering Strait: Annual and interannual variability, *J. Geophys. Res.*, *93*, 15,535–15,539.

Cunningham, S., et al. (2007), Temporal variability of the Atlantic meridional overturning circulation at 26.51°N, *Science*, *317*, 935–938.

de las Heras, M. M., and R. Schlitzer (1999), On the importance of intermediate water flows for the global ocean overturning, *J. Geophys. Res.*, *104*, 15,515–15,536.

Dong, S., S. L. Garzoli, M. O. Baringer, C. Meinen, and G. J. Goni (2009), Interannual variations in the Atlantic meridional overturning circulation and its relationship with the net northward heat transport in the South Atlantic, *Geophys. Res. Let.*, *36*, L20606, doi:10.1029/2009GL039356.

Dong, S., M. O. Baringer, G. J. Goni, C. S. Meinen, and S. L. Garzoli (2014), Seasonal variations in the South Atlantic meridional overturning circulation from observations and numerical models, *Geophys. Res. Lett.*, *41*, 4611–4618, doi:10.1002/2014GL060428.

Dong, S., G. Goni, and F. Bringas (2015), Temporal variability of the South Atlantic meridional overturning circulation between 20°S and 35°S, *Geophys. Res. Lett.*, *42*, 7655–7662, doi:10.1002/2015GL065603.

Ducet, N., P. Y. L. Traon, and G. Reverdin (2000), Global high resolution mapping of ocean circulation from the combination of t/p and ers-1/2, *J. Geophys. Res.*, *105*, 19,477–19,498.

Enfield, D. B., A. M. Mestas-Nunez, and P. J. Trimble (2000), The Atlantic Multidecadal Oscillation and its relation to rainfall and river flows in the continental U.S., *Geophys. Res. Lett.*, *28*, 2077–2080.

Fu, L. L. (1981), The general circulation and meridional heat transport of the subtropical South Atlantic determined by inverse methods, *J. Phys. Oceanogr.*, *11*, 1171–1193.

Ganachaud, A., and C. Wunsch (2003), Large-scale ocean heat and freshwater transports during the World Ocean Circulation Experiment, *J. Clim.*, *16*, 696–705.

Garzoli, S., and M. Baringer (2007), Meridional heat transport determined with expandable bathythermograph, Part II: South Atlantic transport, *Deep Sea Res., Part I*, *54*, 1402–1420.

Garzoli, S., and R. Matano (2011), The South Atlantic and the Atlantic meridional overturning circulation, *Deep Sea Res., Part II*, *58*(17–18), 1837–1847.

Garzoli, S., M. Baringer, S. Dong, R. C. Perez, and Q. Yao (2013), South Atlantic meridional fluxes, *Deep Sea Res., Part I*, *71*, 21–32.

Gordon, A. L. (1985), Indian-Atlantic transfer of thermocline water at the Agulhas Retroflection, *Science*, *227*, 1030–1033.

Gordon, A. L. (1986), Interocean exchange of thermocline water, *J. Geophys. Res.*, *91*, 5037–5046.

Gordon, A. L., and W. F. Haxby (1990), Agulhas eddies invade the South Atlantic: Evidence from GEOSAT altimeter and shipboard conductivity-temperature-depth survey, *J. Geophys. Res.*, *95*, 3117–3125.

Hellermann, S., and M. Rosenstein (1983), Normal monthly wind stress over the world ocean with error estimates, *J. Phys. Oceanogr.*, *13*, 1093–1104.

Hobbs, W. R., and J. K. Willis (2012), Midlatitude North Atlantic heat transport: A time series based on satellite and drifter data, *J. Geophys. Res.*, *117*, C01008, doi:10.1029/2011JC007039.

Holfort, J., and G. Siedler (2001), The meridional oceanic transports of heat and nutrients in the South Atlantic, *J. Phys. Oceanogr.*, *31*, 15–29.

Johns, W. E. (2011), Continuous, array-based estimates of Atlantic ocean heat transport at 26.5°N, *J. Clim.*, *24*(10), 2429–2449.

Kalnay, E., et al. (1996), The NCEP/NCAR 40-year reanalysis project, *Bull. Am. Meteorol. Soc.*, *77*, 437–470.
Kanamitsu, M., W. Ebisuzaki, J. Woollen, S.-K. Yang, J. Hnilo, M. Fiorino, and G. L. Potter (2002), NCEP-DOE AMIP-II reanalysis (r-2), *Bull. Am. Meteorol. Soc.*, *83*(11), 1631–1643.
Locarnini, R. A., et al. (2013), World Ocean Atlas 2013, in *Temperature*, vol. 1, edited by S. Levitus and A. Mishonov, 40 pp., NOAA Atlas NESDIS 73, Silver Spring, Md.
Lopez, H., S. Dong, S. K. Lee, and G. Goni (2016), The role of the South Atlantic Meridional Overturning Circulation variability on modulating interhemispheric atmospheric circulation and monsoons, *J. Clim., 25*(5), 1831–1851, doi:10.1175/JCLI-D-15-0491.1.
Lumpkin, R., and G. C. Johnson (2013), Global ocean surface velocities from drifters: Mean, variance, ENSO response, and seasonal cycle, *J. Geophys. Res. Oceans*, *118*, 2992–3006, doi:10.1002/jgrc.20210.
Mielke, C., E. Frajka-Williams, and J. Baehr (2013), Observed and simulated variability of the AMOC at 26°N, and 41°N, *Geophys. Res. Lett.*, *40*, 1159–1164, doi:10.1002/grl.50233.
McCarthy, G., E. Frajka-Williams, W. E. Johns, M. O. Baringer, C. S. Meinen, H. L. Bryden, D. Rayner, A. Duchez, C. Roberts, and S. A. Cunningham (2012), Observed interannual variability of the Atlantic meridional overturning circulation at 26.5°N, *Geophys. Res. Lett.*, *39*, L19609, doi:10.1029/2012GL052933.
McDonagh, E. L., and B. A. King (2005), Oceanic fluxes in the South Atlantic, *J. Phys. Oceanogr.*, *35*, 109–122.
Meinen, C. S., R. C. P. S. Speich, S. Dong, A. R. Piola, S. L. Garzoli, M. O. Baringer, S. Gladyshev, and E. J. D. Campos (2013), Temporal variability of the Meridional overturning circulation at 34.5°S: Results from two pilot boundary arrays in the South Atlantic, *J. Geophys. Res.*, *118*, 6461–6478, doi:10.1002/2013JC009228.
Richardson, P. L. (2007), Agulhas leakage into the Atlantic estimated with subsurface floats and surface drifters, *Deep Sea Res., Part I, 56*(8), 1361–1389.
Saunders, P. M., and B. A. King (1995), Oceanic fluxes on the WOCE A11 section, *J. Phys. Oceanogr.*, *25*, 1942–1958.
Schmid, C. (2014), Mean vertical and horizontal structure of the subtropical circulation in the South Atlantic from three-dimensional observed velocity fields, *Deep Sea Res., Part I*, *91*(9), 50–71, doi:10.1016/j.dsr.2014.04.015.
Smith, W. H. F., and D. T. Sandwell (1997), Global seafloor topography from satellite altimetry and ship depth soundings, *Science*, *277*, 1957–1962.
Stouffer, R. J., et al. (2006), Investigating the causes of the response of the thermohaline circulation to past and future climate changes, *J. Clim.*, *19*, 1365–1387.
Sutton, R. T., and D. L. R. Hodson (2005), Atlantic Ocean forcing of North American and European summer climate, *Science*, *309*, 115–118, doi:10.1126/science.1109496.
Talley, L. D. (2003), Shallow, intermediate and deep overturning components of the global heat budget, *J. Phys. Oceanogr.*, *33*, 530–560.
Uppala, S., et al. (2005), The era-40 re-analysis, *Q. J. R. Meteorol. Soc.*, *131*, 2961–3012, doi:10.1256/QJ.04.176.
Vellinga, M., and R. A. Wood (2002), Global climatic impacts of a collapse of the Atlantic thermohaline circulation, *Clim. Change*, *54*(3), 251–267.
Willis, J. K. (2010), Can in situ floats and satellite altimeters detect long-term changes in Atlantic ocean overturning?, *J. Geophys. Res.*, *37*, L06602, doi:10.1029/2010GL042372.
Zweng, M. M., et al. (2015), Eddy characteristics in the South Indian Ocean as inferred from surface drifters, *Ocean Sci.*, *11*, 361–371, doi:10.5194/os-11-361-2015.